NASA Technical Memorandum 83692

Three Component Velocity Measurements Using Fabry-Perot Interferometer

Richard G. Seasholtz and Louis J. Goldman
Lewis Research Center
Cleveland, Ohio

Prepared for the
Second International Symposium on Applications
of Laser Anemometry to Fluid Mechanics
sponsored by Instituto Superior Técnico (Lisbon)
Lisbon, Portugal, July 2-4, 1984

NASA

Three Component Velocity Measurements Using Fabry-Perot Interferometer

Richard G. Seasholtz and Louis J. Goldman
National Aeronautics and Space Administration
Lewis Research Center
Cleveland, Ohio 44135

ABSTRACT

A method for measuring the three components of mean flow velocity using a backscatter optical system based on a confocal Fabry-Perot interferometer is described. An analysis of the expected uncertainties in the velocity component measurements is presented along with experimental data taken in a free jet at two flow velocities (100 and 300 m/s).

INTRODUCTION

The measurement of the three components of velocity is needed in many fluid mechanics experiments. Because of its non-intrusive nature, laser anemometry is frequently selected for these measurements. The preferable laser anemometer approach is to measure the three orthogonal velocity components directly (as described by Meyers and Wilkinson, 1982, for example). This generally requires optical access from two orthogonal directions if the usual dual-beam fringe or two-spot techniques are employed. With optical access limited to a single viewing port, other approaches must be considered.

With a single optical viewing port, one approach is to measure non-orthogonal velocity components using backscatter dual-beam fringe optics, such as described by Neti and Clark (1979) and by Johansson (1976). This method offers the advantage of all real-fringe systems — the capability to effectively use scattered light collected over large apertures. Unfortunately, the error of the velocity component along the optical axis derived in this manner becomes large when only components close to the optical axis are measured (Orloff and Snyder, 1982).

Another approach for measuring three velocity components used by Orloff and Logan (1973) is to combine a reference-beam heterodyne technique to obtain the on-axis component with fringe optics to obtain the components normal to the optical axis. One difficulty, however, in using the reference-beam method in high speed flows is that the Doppler frequency shift for backscatter is about 4 MHz/m/s for visible laser light. This results in a dynamic frequency range that can easily exceed the frequency response of most commonly used photomultiplier tubes. Another fundamental limitation of the reference-beam technique is expressed by the Antenna Theorem (Siegman, 1966), which states that the maximum effective aperture area is limited to about λ^2/Ω where Ω is the solid angle subtended by the probe volume at the receiver aperture.

An alternative approach for measuring the component along the optical axis is to directly measure the Doppler shift using an interferometer. In previous work (Seasholtz and Goldman, 1982) we demonstrated the feasibility of using a confocal Fabry-Perot interferometer to measure the line-of-sight velocity component in a flow that is predominantly transverse to the line-of-sight.

The direct measurement of the Doppler shift with a Fabry-Perot interferometer offers advantages in high speed flow experiments compared with the more common dual-beam fringe and reference-beam laser anemometers. One advantage is an essentially unlimited velocity range. Dual-beam fringe and reference beam techniques are limited by the frequency response of the photodetectors and signal processing equipment to a few hundred Megahertz. Another advantage of interferometric measurements is that the amount of usable scattered light is not limited by the Antenna Theorem, but by the light-gathering power (etendue) of the interferometer. This generally allows more of the scattered light to be used.

Other workers have used the Fabry-Perot interferometer for single component measurements in wind tunnels (Jackson and Paul, 1970, 1971; Eggins and Jackson, 1972; Jackson and Eggins, 1976), in rocket exhausts (James, Babcock, and Seifert, 1968; Morse et. al., 1969), and in an MHD generator (Self, 1974).

This paper describes a more general technique suitable for measuring the three components of the mean flow velocity using a confocal Fabry-Perot interferometer (CFP). A backscatter optical configuration is described that can be operated in two modes. The first mode uses a single beam offset from the optical axis with the scattered light collected along the optical axis. The second mode is a dual-beam configuration using optics similar to those in a dual-beam fringe system.

In the dual-beam mode, the CFP can measure two orthogonal velocity components with a single orientation of the input beams. The components measured are the component along the optical axis and one component normal to the optical axis. Rotation of the plane of the two input beams allows the third velocity component to be measured.

An analysis of the expected uncertainties in the velocity measurements is presented along with experimental results for a small free jet operated at two velocities (100 m/s and 300 m/s).

In this paper, the following terminology will be used: a conventional dual-beam fringe-type laser anemometer using a counter-type signal processor will be referred to as a "fringe" anemometer; a reference-beam heterodyne anemometer will be referred to as a "reference-beam" anemometer; and an anemometer based on the direct measurement of Doppler shift using a confocal Fabry-Perot interferometer will be referred to as a "Fabry-Perot", or "CFP", anemometer.

APPARATUS

Optical System

The layout of the optical system is shown in Figure 1. An argon-ion laser was equipped with an etalon and produced 0.2 W single-frequency output at 514.5 nm. After the beam passed through the colli-

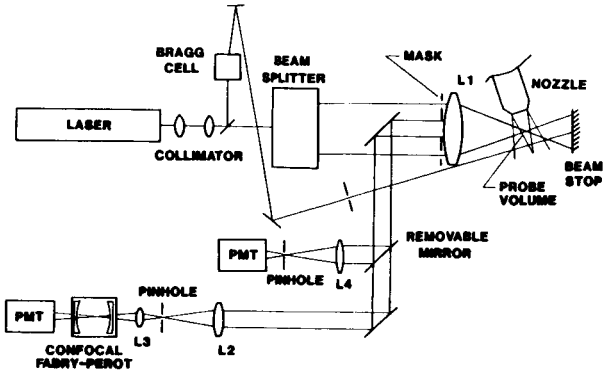

Figure 1.- Optical configuration for three component measurements using Fabry-Perot Interferometer.

mator (adjusted to position the beam waist at the focal point of lens L1), the beam was split into two equal intensity beams with an 82 mm separation. The beam splitter was assembled from commercially available optical modules incorporating a rotary mount so that the orientation of the beams could be easily adjusted. The system could be operated in the dual-beam mode or in a single beam mode by blocking one of the beams. The beam(s) were focused by lens L1 (f/2.5, 250 mm focal length) in the probe volume (dia. about 30 μm). The fringe spacing (with the dual beams) was determined (by measuring the crossing angle of the beams $2\beta = 18.86^\circ$) to be 1.57 μm. The light scattered by particles in the flow passing through the probe volume was collected by lens L1 and masked by a 25 mm diameter aperture located on the optical axis.

The scattered light, after being reflected by two mirrors, was focused by lens L2 (160 mm focal length) onto a pinhole aperture (diameter 50 μm). A 10X microscope objective L3 was placed to form an image of the pinhole (and hence the probe volume) at the central plane of the CFP. (A description of the theory of the CFP is given by Hercher (1968)). The magnified image of the probe volume was about 0.2 mm diameter. Since the receiving optics aperture restricted the angular divergence of light from the probe volume to 5.7°, the angular divergence at the CFP was 0.89°.

The CFP had a mirror separation d = 25 mm giving a free spectral range of 3 GHz. The actual spacing is electrically adjustable over a small range by means of a piezo-electric element, allowing the CFP to be used as a scanning optical spectrum analyser.

A collimated beam of monochromatic light incident along the axis of the CFP will form a multiple beam interference pattern in the central plane of the interferometer (Hercher, 1968). With the mirror separation at a resonance condition the diameter of the central fringe is

$$D_S = 2(d^3\lambda/F)^{1/4} \qquad (1)$$

where F is the instrument finesse defined as the ratio of the free spectral range to the observed instrumental bandwidth (full-width at half-maximum). The measured finesse was F = 60. The transmittance function of the CFP for an aperture small compared to D_S is the Airy function

$$T(f,d) = T_0/(1 + (2F/\pi)^2 \sin^2(4\pi df/c)) \qquad (2)$$

where T_0 is the maximum transmittance (about 0.1) and c is the velocity of light.

The measure of an instrument's light-gathering power is the etendue U defined as

$$U = A\,\Omega \qquad (3)$$

where A is the aperture area and Ω is the solid angle of the field of view subtended at the aperture.

For a CFP both A and Ω have an upper limit that cannot be exceeded without degrading the effective finesse. These limits, here designated A_S and Ω_S, are

$$A_S = \pi D_S^2/4 = 1.15 \times 10^{-6}\ m^2 \qquad (4)$$

$$\Omega_S = \pi\theta_S^2/4 = A_S/d^2 = 1.84 \times 10^{-3}\ sr \qquad (5)$$

The maximum light-gathering power (etendue) of the CFP is thus

$$U = A_S\Omega_S = \pi^2 d\lambda/F = 2.12 \times 10^{-9}\ sr\text{-}m^2 \qquad (6)$$

For the optical parameters used in this work, the probe volume image area was 2.9×10^{-8} m^2, and the solid angle of the scattered light entering the CFP was 1.9×10^{-4} sr. Thus both the image area and solid angle are less than the maximum allowable values. The etendue of this system was 1.5×10^{-11} $sr\text{-}m^2$, which is much smaller than the maximum given by Equation 6. This indicates that much more of the scattered light could have been used, which would have significantly increased the signal-to-noise ratio. Note that this configuration, which only used a fraction of the maximum light-gathering power of the CFP, still uses much more of the scattered light than would be possible with a reference-beam system. (The maximum light-gathering power of a reference-beam system, as given by the Antenna Theorem, is $\lambda^2 = 2.7 \times 10^{-13}$ $sr\text{-}m^2$.)

In the dual-beam configuration, the system may be operated as a fringe-type anemometer. As shown in Figure 1, the removable mirror may be used to direct the scattered light to lens L4, which focuses the light onto 100 μm diameter pinhole aperture mounted on a PMT. A commercial counter-processor interfaced to the computer is used to measure the velocity component normal to the optical axis.

The system also included an acousto-optic modulator (Bragg cell) to generate a reference signal offset from the laser frequency. This reference beam was directed to a surface on the optical axis so some of the scattered light would reach the photodetector.

Electronics and Data Acquisition

A linear ramp generator that produced a sawtooth waveform with adjustable period, amplitude, and offset was used to scan the CFP over the desired frequency range.

The CFP spectral measurements were made by scanning over a frequency range less than the free spectral range to reduce the data acquisition time. Some unshifted light and some light shifted by a Bragg cell were used to calibrate the output spectrum. The photomultiplier signal was processed with photon counting electronics that accumulated the number of photon counts for a preset time interval equal to 1/256 of the ramp period. These counts were sent to a small laboratory computer, which stored them in the form of a 256 bin histogram.

A digital storage oscilloscope synchronized with the ramp generator was used to continuously monitor the analog output of the photon counter. This gave the operator a real-time picture of the spectrum being accumulated in the computer.

MEASUREMENT THEORY

Scattering Theory

Consider a plane wave with wave vector $\underline{k}_{oi}$ incident on a particle moving with velocity $\underline{V}$ as shown in Figure 2. Light scattered with wave vector $\underline{k}_S$ will be Doppler shifted by an amount

$$f_i = f_s - f_o = (1/2\pi)\,(\underline{k}_s - \underline{k}_{oi})\cdot\underline{V} \qquad (7)$$

where f_o and f_s are the frequencies (Hz) of the incident and scattered waves respectively. If we assume that $|\underline{k}_{oi}| = |\underline{k}_s| = k = 2\pi/\lambda$ (a good

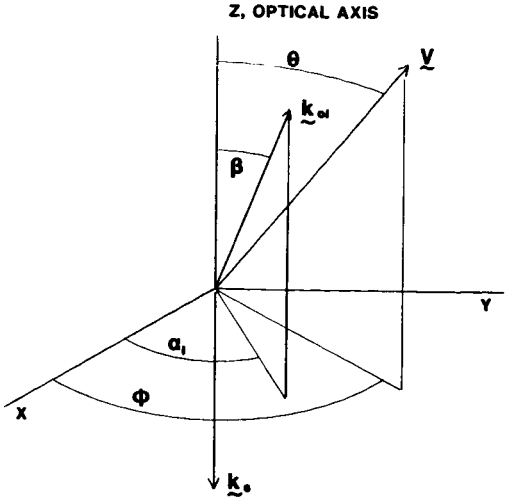

Figure 2.- Vector diagram showing incident beam $\underset{\sim}{k}_{oi}$, scattered beam $\underset{\sim}{k}_s$, and velocity $\underset{\sim}{V}$; the spherical coordinate system is used.

approximation for particle velocities much less than the velocity of light), then the vector $(\underset{\sim}{k}_s - \underset{\sim}{k}_{oi})$ lies on the bisector of $\underset{\sim}{k}_s$ and $-\underset{\sim}{k}_{oi}$.

If the scattering wave vector $\underset{\sim}{k}_s$ lies along the -z axis and the incident wave propagation direction is described by the angles α_i and β shown in Figure 2, the Doppler shift given by Equation 7 may be written

$$f_i = -(V/\lambda)[\sin\theta \sin\beta \cos(\phi - \alpha_i) + \cos\theta (1+\cos\beta)] \quad (8)$$

In general, three independent measurements (at 3 values of α_i) will allow the determination of the three components of the velocity.

Instead of using only three measurements to determine the vector velocity, it is often preferable to use the method of least squares (Wolberg, 1967) with more than three measurements to calculate the velocity components along with estimates of their uncertainties.

Prediction of Measurement Uncertainties

The use of prediction analysis allows the experimenter to obtain estimates of the expected uncertainties in a least squares analysis of the data before the experiment is conducted. Here, we apply this technique to find the expected uncertainty in the measurement of velocity using the Fabry-Perot interferometer.

The expected uncertainty in a parameter a_k is given by the square root of the diagonal components of the inverse C matrix (Wolberg, 1967, pp. 75-82)

$$\sigma_{a_k} = \sqrt{(C^{-1})_{kk}} \quad (9)$$

where the C matrix has components

$$C_{kl} = \sum_i \frac{1}{L_i} \frac{\partial f_i}{\partial a_k} \frac{\partial f_i}{\partial a_l} \quad (10)$$

In Equation 10, the f_i are given by Equation 8; the a_k are the parameters V, θ, and ϕ; and the L_i are weighting factors given by

$$L_i = \sigma_{f_i}^2 + \left(\frac{\partial f_i}{\partial \alpha_i} \sigma_{\alpha_i}\right)^2 \quad (11)$$

where σ_{α_i} are the uncertainties in the measurements of the independent variable α_i, and σ_{f_i} are the uncertainties in the measurements of the dependent variable f_i.

To obtain analytical expressions for the C matrix elements, we assume n equally spaced values of α_i over the range 0 to 2π. The summation in Equation 10 is converted to an integral and the C matrix components are found to be

$$\begin{aligned}
C_{11} &= (n/\lambda^2\sigma_f^2)[(1/2)\sin^2\theta \sin^2\beta + \cos^2\theta(1+\cos\beta)^2] \\
C_{22} &= (V^2 n/\lambda^2\sigma_f^2)[(1/2)\cos^2\theta \sin^2\beta + \sin^2\theta(1+\cos\beta)^2] \\
C_{33} &= (V^2 n/2\lambda^2\sigma_f^2) \sin^2\theta \sin^2\beta \\
C_{12} &= C_{21} = -(Vn/\lambda^2\sigma_f^2) \sin\theta\cos\theta [(1/2)\sin^2\beta - (1+\cos\beta)^2] \\
C_{13} &= C_{31} = C_{23} = C_{32} = 0
\end{aligned} \quad (12)$$

where σ_f^2 is the variance in the measurement of the frequency f. Here we assumed that $\sigma_{f_i} = \sigma_f$ is the same for all measurements and that there is no uncertainty in the independent variable α_i (i.e., $\sigma_{\alpha_i} = 0$).

Evaluation of Equation 9 using the C matrix elements given in Equations 12 gives the uncertainties in the velocity parameters (V, θ, ϕ)

$$\begin{aligned}
\sigma_V &= \sqrt{2/n}(\lambda\sigma_f)\sqrt{(1/2)\cos^2\theta\sin^2\beta + \sin^2\theta(1+\cos\beta)^2} \\
&\quad \div [\sin\beta(1+\cos\beta)] \\
\sigma_\theta &= \sqrt{2/n}(\lambda\sigma_f/V)\sqrt{(1/2)\sin^2\theta \sin^2\beta + \cos^2\theta(1+\cos\beta)^2} \\
&\quad \div [\sin\beta(1+\cos\beta)] \\
\sigma_\phi &= \sqrt{2/n}(\lambda\sigma_f)/[V \sin\theta \sin\beta]
\end{aligned} \quad (13)$$

Note that σ_ϕ is undefined for the flow directly along the optical axis.

Two special cases can be easily evaluated to show the expected uncertainties for V and θ. The first case is for the flow normal to the optical axis ($\theta = 90°$) where

$$\begin{aligned}
\sigma_V &= \sqrt{2/n}\ (\lambda\sigma_f)/\sin\beta \\
\sigma_\theta &= \sqrt{1/n}\ (\lambda\sigma_f)/[V(1+\cos\beta)]
\end{aligned} \quad (14)$$

The second special case is for the flow along the optical axis ($\theta = 0°$) where

$$\begin{aligned}
\sigma_V &= \sqrt{1/n}\ (\lambda\sigma_f)/(1+\cos\beta) \\
\sigma_\theta &= \sqrt{2/n}\ (\lambda\sigma_f)/(V \sin\beta)
\end{aligned} \quad (15)$$

To illustrate the application of this prediction analysis, we consider the following example:

(1) velocity magnitude V = 300 m/s
(2) no uncertainty in angle α_i, i.e., $\sigma_{\alpha_i} = 0$
(3) uncertainty in measurement of Doppler shift, σ_f= 3 MHz
(4) 8 measurements made at equal spacing over 360°
(5) laser wavelength λ = 0.5 μm
(6) angle between incident beam and optical axis $\beta = 10°$

From equations 14 and 15 the uncertainties in the measurement are

	$\theta = 90°$	$\theta = 0°$
σ_V	4.3 m/s	0.3 m/s
σ_θ	0.1°	0.8°
σ_ϕ	0.8°	----

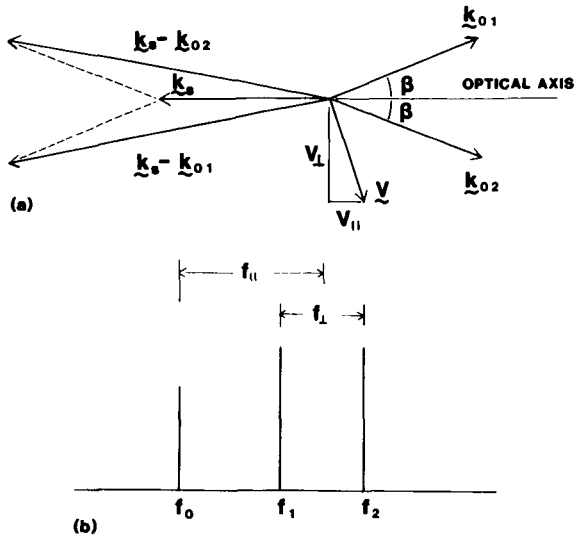

Figure 3.- Dual-beam configuration (a) wave vector diagram showing incident beams $\underset{\sim}{k}_{o1}$ and $\underset{\sim}{k}_{02}$, scattered beam $\underset{\sim}{k}_S$, velocity $\underset{\sim}{V}$(b) spectral components, $f_\perp$ is proportional to tranverse velocity component and $f_\parallel$ is proportional to component along the optical axis.

Note that the uncertainty in the magnitude of the velocity is a strong function of the beam angle and that it is much greater for the flow normal to the optical axis. This is a result of the measured Doppler shift frequencies being a measure of velocity components close to the optical axis. Recall that this is the opposite situation one encounters with fringe type anemometers where the component along the optical axis is measured with less accuracy than the components normal to the optical axis (Neti and Clark, 1979).

Dual-Beam Configuration

With the dual-beam configuration two orthogonal velocity components may be measured from a single spectrum. If the scattered light wave vector $\underset{\sim}{k}_S$ is along the optical axis and the two incident beams are symmetrically located about the optical axis (Fig. 3), the average and difference of the Doppler shift frequencies of the two scattered beams are proportional to the velocity components along and perpendicular to the optical axis, respectively. That is,

$$f_\perp = f_2 - f_1 = (1/2\pi)(\underset{\sim}{k}_{o1} - \underset{\sim}{k}_{o2})\cdot\underset{\sim}{V} = V_\perp / s_\perp$$
$$f_\parallel = [(f_2 - f_o) + (f_1 - f_o)]/2 = V_\parallel / s_\parallel \quad (16)$$

where, $s_\perp = \lambda/(2\sin\beta)$
$s_\parallel = \lambda/(1+\cos\beta)$ (17)

Note that $s_\perp$ is the usual fringe spacing of the fringe anemometer.

With this dual-beam configuration, two spectra taken at two orientations of the real-fringe pattern (as measured by the angle α_i) are needed to determine the vector velocity.

Hybrid Mode

The dual-beam configuration may also be used in a hybrid mode where the transverse velocity components are measured using conventional fringe signal processing techniques, and the on-axis component is measured with the CFP . For this hybrid mode, the removable mirror shown in Figure 1 would be replaced by a beam splitter.

The hybrid mode is preferable if the velocities are low enough so that the frequencies are within the bandwidth of the photodetector and signal processor. This mode may also be used with a fluorescent dye as the seed material (Stevenson, dos Santos, and Mettler, 1975). The fluorescence would be used to measure the transverse component and the part of the light at the incident wavelength would be used for the CFP measurement of the line-of-sight component. The advantage of using the laser induced fluorescence is that measurements may be made near surfaces.

Spectral Broadening

In addition to the inherent instrumental bandwidth of the CFP, there are three additional factors that cause broadening of the spectral line of the light scattered by particles moving through the probe volume. One factor is fluctuations (jitter) in the laser frequency. In a controlled laboratory environment this is about • 10 MHz for time periods on the order of seconds, but will be larger for high acoustic noise or high vibration environments. This jitter in the laser frequency, of course, likewise affects the reference and non-Doppler shifted frequencies.

A second reason for spectral broadening is the range of scattering angles caused both by the angular spectrum of the incident beam, which can also be thought of as transit time broadening, and by the range of scattered light wave vectors accepted by the receiving optics.

The standard deviation of the spectral broadening due to the incident beam is (Edwards et. al., 1971)

$$\Delta f_B = V_\perp/(\pi d_o) \quad (18)$$

where $V_\perp$ is the transverse velocity component and d_o is the diameter of the probe volume. The standard deviation of the broadening due to the receiving optics aperture is

$$\Delta f_R = V_\perp \theta_R/(4\lambda) \quad (19)$$

where θ_R is the angle subtended by the receiver aperture at the probe volume.

The third cause of spectral broadening is fluctuations in the frequency corresponding to fluctuations in the velocity component along the optical axis (i.e. the turbulence). This provides a means of using the spectral width to calculate this component of the turbulence intensity provided that the other broadening effects are smaller.

EXPERIMENTAL RESULTS

Two sets of measurements were made in a small free jet. One set was made with a velocity magnitude of about 100 m/s using the single beam configuration. The second set of measurements was made at sonic flow conditions.

The free jet had a 8.9 mm exit diameter and was operated from the laboratory compressed air supply. The exit was at ambient pressure. All measurements were made 4 mm from the exit plane on the centerline of the jet. The flow angle of the jet relative to the optical axis was set at approximately 70°, which corresponded to a component along the optical axis of 34 percent of the velocity magnitude. This assured that the Doppler shifted spectral peak did not overlap the unshifted peak. The velocity magnitude was determined by measuring the total temperature and total pressure and assuming isentropic flow through the nozzle. A mineral oil aerosol was injected upstream of the nozzle to provide seed particles.

The CFP spectral measurements were made by scanning over a frequency range less than the free spectral range to reduce the data acquisition time. The scan time was 4 seconds. The known Bragg cell frequency was used to calibrate the CFP spectrum. The Doppler shift frequencies are then determined using nonlinear least square parameter estimation techniques (Wolberg, 1967, Chap. 3) that provide both estimates of the Doppler shift and the error in the

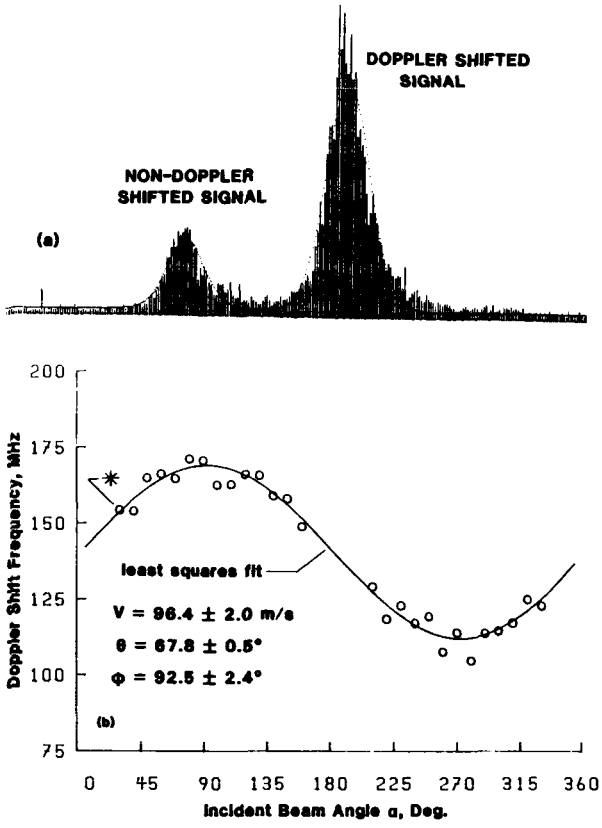

Figure 4.- Low velocity free jet Fabry-Perot data (a) single beam spectrum at α_i = 30° with least squares fit shown as dotted line (b) Doppler frequency shift data and least squares fit; the * indicates the datum taken from the spectrum shown in part (a).

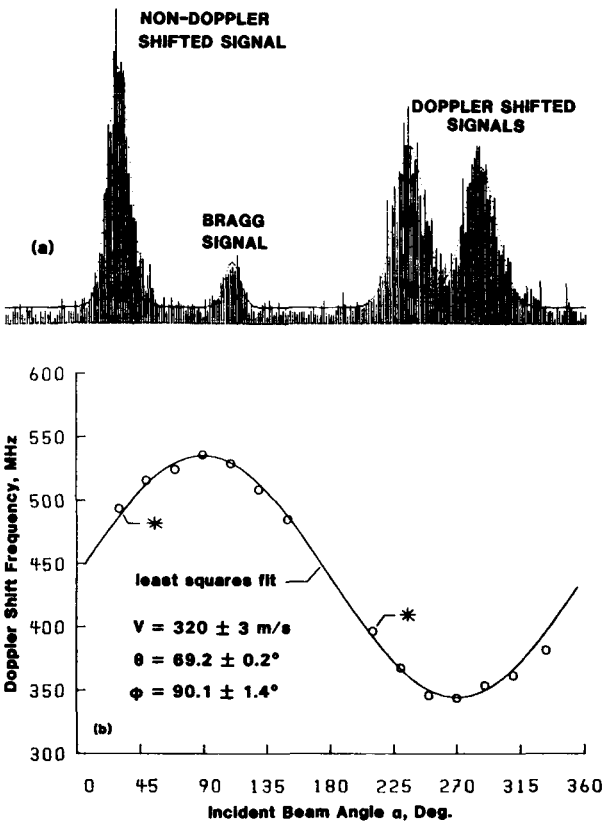

Figure 5.- Sonic velocity free jet Fabry-Perot data (a) dual-beam spectrum at α_i = 30°, 210° with least squares fit shown as dotted line (b) Doppler shift data and least squares fit; the * indicate the data taken from the spectrum shown in part (a).

estimate. The spectral peaks were modeled as Gaussian functions plus a constant, and Poisson statistics were assumed. The frequencies of the peaks were then used to determine the mean velocity magnitude V and direction angles θ and ϕ; again using least squares parameter estimation with Equation 8 as the model function.

Low Velocity Measurements

The single beam technique was used to measure spectra at 27 values of the angle α_i. A typical spectrum with the least squares fit is shown in Figure 4a for α_i= 30°. The left peak is caused by the unshifted laser light and the right peak is due to light scattered from the seeded flow. The spectrum calibration factor was measured using the third order Bragg diffracted beam (116.5 MHz). Figure 4b shows the Doppler shift as a function of the angle of the incident beam α_i along with the least squares fit. The velocity magnitude and direction determined from the least squares fit were V = 96.4 ± 2.0 m/s, θ = 67.8° ± 0.5°, and ϕ = 92.5° ± 2.4°. The statistical error bounds correspond to one standard deviation.

The velocity magnitude calculated from the measured total temperature and total pressure was 102.1 m/s. Measurements were also taken using the dual-beam configuration and the counter-processor. The measured transverse velocity component was 94.2 m/s; the velocity magnitude calculated from this component and the flow angle measured with the CFP was 101.7 m/s. The apparent systematic error in the CFP measurements is believed to be caused by an error in the calibration constant as explained in the Discussion of Results section.

Sonic Velocity Measurements

For these measurements, the jet was operated at sonic flow. Because the nozzle mounting hardware was changed between tests, the orientation of the jet was not identical to the orientation in the low velocity measurements. The CFP measurments were made using the dual-beam optical configuration. A typical spectrum is shown in Figure 5a for the incident beam angles of 30° and 210°. The calibration constant was determined for each spectrum using the unshifted peak (the left peak) and the fourth order (155.4 MHz) Bragg diffracted peak, (the next to left peak). The right two peaks are due to Doppler shifted light scattered from the seed particles in the jet. Seven spectra were taken and used to calculate the least squares fit shown in Figure 5b. (Each spectrum contributed two Doppler shift frequencies, corresponding to the light scattered from the two incident beams.) The velocity magnitude and direction determined from the least squares fit were V = 320 ± 3 m/s, θ = 69.2° ± 0.2°, and ϕ = 90.1° ± 1.4°.

The velocity calculated from the total temperature was 313 m/s. As with the low velocity measurements, the velocity magnitude calculated from the pressure and temperature measurements was outside the statistical error bounds of the CFP measurements.

Discussion of Results

For both measurements described above, the CFP measurements of the velocity magnitude did not agree with the value determined from the total temperature and pressure measurements. (The velocity calculated using the isentropic flow relations for the velocity as a function of total temperature and pressure is believed accurate to at least one percent.) The CFP errors were more than could be accounted for by statistical errors, an indication of systematic errors. This apparent systematic error in the CFP measurements is believed to be caused by errors in the measurement of the calibration factor of the spectra.

It was observed that the measured calibration factor tended to change with time. Since the Bragg cell frequency was constant, this change was probably caused by either a drift in the ramp voltage that was used to scan the CFP, or by a change in the relation between the piezo-electric element displacement and the applied voltage.

In the first set of data (the low velocity measurements), the calibration factor was measured separately from the velocity data. Two measurements of the calibration factor were used. Over the course of the measurements, the calibration factor changed by about 8 percent. This change could account for the apparent systematic error of 6 percent.

In the second set of data (the sonic velocity measurements), the calibration factor was determined from each spectrum, thus eliminating the drift problems encountered in the low velocity measurements. However, the frequency spacing of the spectral peaks used for the calibration was only about one-third of the Doppler shift frequencies. This means that an one percent error in the calibration would result in a three percent error in the Doppler frequency measurement. This could easily account for the two percent error in the velocity magnitude measurement.

To reduce errors in the calibration factor measurement, the Bragg cell frequency should be selected so that the spacing of the spectral calibration peaks is at least as large as the Doppler shift frequencies. Also, the calibration should be determined for each spectrum (as was done for the sonic velocity measurements).

CONCLUDING REMARKS

In this paper it was shown that a Fabry-Perot interferometer can be used to measure the three components of velocity using a backscatter optical configuration. Because the velocity component measured with a Fabry-Perot lies approximately along the line-of-sight, this component can be more easily measured than with a fringe system. However, the transverse components are measured with less accuracy. In this sense the interferometric systems (along with reference-beam heterodyne systems) are complementary to the fringe systems. To obtain accurate three component measurements with either system requires a fairly large viewing cone (about f/3 or larger). With limited optical access, one is led to consider hybrid techniques that combine the fringe method with either reference-beam or interferometric methods. Interferometric methods are more suitable with high velocity flows because of lack of any limitations on the measurable Doppler frequency shift.

One final consideration that should be mentioned is that interferometric laser anemometry techniques, such as described in this paper, require that the laser frequency have only a small amount of jitter. This is usually not a problem in laboratory environments, but in test facilties that generate high levels of mechanical vibration and/or acoustic noise levels the laser may exhibit an unacceptable amount of frequency jitter. In previous work conducted in a turbine stator cascade facilty (Seasholtz and Goldman, 1982), it was necessary to locate the laser and optics in an acoustic enclosure. This problem of frequency stability is generally not a problem with fringe-type anemometers.

REFERENCES

Edwards, R. V. Angus, J. C., French, M. J., and Dunning, J. W., Jr., 1971, "Spectral Analysis of the Signal from the Laser Doppler Flowmeter: Time-Independent Systems", J. Appl. Phys., 42, 837.

Eggins, P. L., and Jackson, D. A., 1972, "Laser Doppler Velocity Measurements in Supersonic Flow without Artificial Seeding", Phys. Lett., 42A, 122.

Hercher, M., 1968, "The Spherical Mirror Fabry-Perot Interferometer", Appl. Opt., 7, 951.

Jackson, D. A., and Paul, D. M., 1970, "Measurement of Hypersonic Velocities and Turbulence by Direct Spectral Analysis of Doppler Shifted Laser Light", Phys. Lett., 32A, 77.

Jackson, D. A., and Paul, D. M., 1971, "Measurement of Supersonic Velocity and Turbulence by Laser Anemometry", J. Phys. E:, 4, 173.

Jackson, D. A., and Eggins, P. L., 1976, "Supersonic Velocity and Turbulence Measurements Using a Fabry-Perot Interferometer", in Application of Non-Intrusive Instrumentation in Fluid Flow Research, AGARD CP-193, pp. 6-1 to 6-13.

James, R. N., Babcock, W. R., and Seifert, J. S., 1968, "Laser-Doppler Technique for the Measurement of Particle Velocity", AIAA J., 6, 160.

Johansson, T. G.,Jernquist, L. F., Karlsson, S. K. F., and Froessling, N., 1976, "A Three-Component Laser-Doppler-Velocimeter", in Applications of Non-Intrusive Instrumentation in Fluid Flow Research, AGARD CP-193, pp. 28-1 to 28-4.

Meyers, J. F., and Wilkinson, S. P., 1982, "A Comparison of Turbulence Intensity Measurements Using a Laser Velocimeter and a Hot Wire in a Low Speed Jet Flow", International Symposium on Applications of Laser-Doppler Anemometry to Fluid Mechanics", pp. 17.4-1 to 17.4-14.

Morse, H. L., Tullis, B. J., Seifert, H. S., and Babcock, W., 1969, "Development of a Laser-Doppler Particle Sensor for the Measurement of Velocities in Rocket Exhausts", J. Space Rockets, 6, 264.

Neti, S., and Clark, W., 1979, "On-Axis Velocity Component Measurement with Laser Velocimeters", AIAA J., 17, 1013.

Orloff, K. L., and Logan, S. E., 1973, "Confocal Backscatter Laser Velocimeter with On-Axis Sensitivity", Appl. Opt., 12. 2477.

Orloff, K. L., and Snyder, P. K., 1982, "Laser-Doppler Anemometer Measurements Using Nonorthogonal Velocity: Error Estimates", Appl. Opt., 21, 339.

Seasholtz, R. G., and Goldman, L. J., 1982, "Laser Anemometer Using a Fabry-Perot Interferometer for Measuring Mean Velocity and Turbulence Intensity Along the Optical Axis in Turbomachinery", in Engineering Applications of Laser Velocimetry, (ed. H. W. Coleman and P. A. Pfund), pp. 93-101. New York: American Society of Mechanical Engineers.

Self, S. A., 1974, "Laser-Doppler Velocimetry in MHD Boundary Layers", in Engineering Aspects of Magnetohydrodynamics (ed. Y. C. L. Wu) pp. V.8.1-V.8.4, University of Mississippi.

Siegman, A. E., 1966, "The Antenna Properties of Optical Heterodyne Receivers", Proc. IEEE, 54, 1350.

Stevenson, W. H., dos Santos, R., and Mettler, S. C., 1975, "A Laser Velocimeter Utilizing Laser-Induced Fluorescence", Appl. Phys. Lett., 27, 395.

Wolberg, J. R., 1967, Prediction Analysis, Princeton, New Jersey, D. Van Nostrand.

1. Report No.	2. Government Accession No.	3. Recipient's Catalog No.
NASA TM-83692		

4. Title and Subtitle	5. Report Date
Three Component Velocity Measurements Using Fabry-Perot Interferometer	6. Performing Organization Code: 505-31-52

7. Author(s)	8. Performing Organization Report No.
Richard G. Seasholtz and Louis J. Goldman	E-2148
	10. Work Unit No.

9. Performing Organization Name and Address	11. Contract or Grant No.
National Aeronautics and Space Administration Lewis Research Center Cleveland, Ohio 44135	13. Type of Report and Period Covered: Technical Memorandum

12. Sponsoring Agency Name and Address	14. Sponsoring Agency Code
National Aeronautics and Space Administration Washington, D.C. 20546	

15. Supplementary Notes

Prepared for the Second International Symposium on Applications of Laser Anemometry to Fluid Mechanics sponsored by Instituto Superior Técnico (Lisbon), Lisbon, Portugal, July 2-4, 1984.

16. Abstract

A method for measuring the three components of mean flow velocity using a backscatter optical system based on a confocal Fabry-Perot interferometer is described. An analysis of the expected uncertainties in the velocity component measurements is presented along with experimental data taken in a free jet at two flow velocities (100 and 300 m/s).

17. Key Words (Suggested by Author(s))	18. Distribution Statement
Laser anemometry Velocity measurement Fabry-Perot interferometer	Unclassified - unlimited STAR Category 35

19. Security Classif. (of this report)	20. Security Classif. (of this page)	21. No. of pages	22. Price*
Unclassified	Unclassified		

*For sale by the National Technical Information Service, Springfield, Virginia 22161